Spectrochimica Acta Part A 79 (2011) 873–883

Contents lists available at ScienceDirect

Spectrochimica Acta Part A: Molecular and Biomolecular Spectroscopy

journal homepage: www.elsevier.com/locate/saa

Metallation of ethylenediamine based Schiff base with biologically active Cu(II), Ni(II) and Zn(II) ions: Synthesis, spectroscopic characterization, electrochemical behaviour, DNA binding, photonuclease activity and *in vitro* antimicrobial efficacy

N. Raman*, A. Selvan, S. Sudharsan

Research Department of Chemistry, VHNSN College, Virudhunagar, Tamil Nadu 626 001, India

ARTICLE INFO

Article history:
Received 23 December 2010
Received in revised form 17 February 2011
Accepted 9 March 2011

Keywords:
Metal complexes
DNA interaction
Photonuclease activity
CT DNA
Antimicrobial activity

ABSTRACT

A new ligand $[C_{28}H_{20}N_6O_8]$ (**L_2**) has been synthesized by the condensation reaction of 3-hydroxy-4-nitrobenzaldehydenephenylhydrazine (**L_1**) with diethyloxalate. This ligand **L_2** is allowed to react with bis(ethylenediamine)Cu(II)/Ni(II)/Zn(II) complexes. It affords $[(L_2)Cu(en)_2]Cl_2$(**1**)/$[(L_2)Ni(en)_2]Cl_2$(**2**)/$[(L_2)Zn(en)_2]Cl_2$(**3**) complexes, respectively. These complexes (**1**–**3**) have been characterized by the spectral and analytical techniques. The interaction of these complexes with calf thymus (CT) DNA is characterized by the absorption spectra which exhibit a slight red shift with hypochromic effect. Electrochemical analyses and viscosity measurements have also been carried out to determine the mode of binding. The shift in ΔEp, $E_{1/2}$ and Ipc values explores the interaction of CT DNA with the above metal complexes. The slight increase in the viscosity of CT DNA indicates that these complexes bind to CT DNA through a partial non-classical intercalative mode. Cleavage experiments using pBR322 DNA in presence of H_2O_2 indicate that these complexes behave as efficient artificial chemical nucleases in the order of **1** > **2** > **3**. Moreover, the antibacterial and antifungal studies reveal that complex **1** is highly active against the bacterial and fungal growth.

1. Introduction

The design of metal–drug complexes is of particular interest in the pharmacological research. Metal combinations with pharmaceutical agents are known to improve the activity of the drugs and decrease their toxicity [1]. Schiff bases are potential anticancer drugs and when administered as their metal complexes, the anticancer activity of these complexes has been enhanced in comparison to the free ligand. Schiff base complexes are considered to be the most important stereochemical models in transition metal coordination chemistry due to their preparative accessibility and structural variety. It has been suggested that the azomethine linkage in Schiff bases is responsible for the biological activities such as antitumor, antibacterial, antifungal and herbicidal activities [2].

A more precise understanding of the DNA-binding properties of metal complexes has come about as a result of numerous motivating factors and developments, including new therapeutic approaches, exhaustive studies of nucleic acid conformations and new tools for nanotechnology [3]. Drug researches suggest that many anticancer, antiviral and antiseptic agents take action by binding to DNA because the interaction between small molecules and DNA can often cause DNA damage in cancer cells resulting in cell death. Many studies indicate that the transition metal complexes can interact non-covalently with DNA by intercalation, groove binding or external electrostatic binding [4].

The development of artificial nucleases is an important aspect of biotechnology, drug designing and molecular biology. Chemical nucleases can cleave DNA by oxidative, photo-induced and hydrolytic processes. Transition metal complexes have been extensively studied for their nuclease-like activity using the redox properties of the metal and dioxygen to produce reactive oxygen species to promote DNA cleavage yielding direct strand scission or base modification. However, these oxidative cleaving agents require an external agent (light, oxidative and/or reductive agent) to initiate cleavage. The hydrolytic cleavage of DNA requires neither additives nor photo-induced irradiation but follows a mechanistic pathway to target the phosphodiester bonds linking the nucleosides, and the cleaved products can be amenable to further enzymatic religation. Among several types of transition metal complexes used as synthetic hydrolases, copper(II) and zinc(II) complexes are better suited for the hydrolysis of DNA due to the strong Lewis acid properties of these metal ions.

Bearing these facts in our mind, herein we report the synthesis and characterization of a new Schiff base derived from the mono-condensation of ethylenediamine with carbonyl compound having a group of NNNN donor site and its different mononuclear

* Corresponding author. Tel.: +91 092451 65958; fax: +91 4562 281338.
E-mail address: drn_raman@yahoo.co.in (N. Raman).

1386-1425/$ – see front matter © 2011 Elsevier B.V. All rights reserved.
doi:10.1016/j.saa.2011.03.017

complexes. Here, our aim is to establish a comparative electrospectrochemical study on the new Schiff-base mononuclear metal complexes with NNNN donor sites. Additionally, a comparative study of the interaction of the complexes **1**–**3** with DNA has been employed in order to investigate the potential mechanism of their biological properties. Moreover, the antibacterial and antifungal activities of these compounds have been carried out against four bacteria and four fungi using DMSO as negative control.

2. Experimental

2.1. Materials and measurements

Phenylhydrazine, diethyloxalate and 3-hydroxy-4-nitrobenzaldehyde were purchased from Aldrich Chemical Company. Ethidium bromide (EB), CT-DNA and pBR322 plasmid DNA were obtained from Sigma. All other chemicals used were of analytical grade. All the experiments involved in the interaction of metal complexes with CT DNA were carried out in doubly distilled water buffer containing 5 mM Tris [tris(hydroxymethyl)-aminomethane] and 50 mM NaCl, adjusted to pH 7.2 with hydrochloric acid. Solution of CT DNA in Tris–HCl buffer gave ratio of UV absorbance of about 1.8–1.9:1 at 260 and 280 nm indicating that the CT DNA was sufficiently free of protein [5]. The CT DNA concentration per nucleotide was determined spectrophotometrically by employing an extinction coefficient of 6600 M^{-1} cm^{-1} at 260 nm [6].

UV–Vis spectra were recorded on a Shimadzu Model 1601 UV–Visible Spectrophotometer. IR spectra of the ligand and its metal complexes were recorded on a Perkin-Elmer FTIR-1605 spectrophotometer using KBr discs. ^{1}H NMR spectra were measured on a Bruker Avance DRX 300 FT-NMR spectrometer with tetramethylsilane (TMS) as the internal standard at room temperature. The complexes were analyzed for their metal contents, following standard procedures [7] after decomposition with a mixture of conc. HNO_3 and HCl, followed by conc. H_2SO_4. Microanalyses (C, H and N) were carried out on a Perkin-Elmer 240 elemental analyzer. Mass spectrometry experiments were performed on a JEOL-AccuTOF JMS-T100LC mass spectrometer equipped with a custom-made electrospray interface (ESI). The X-band EPR spectra of the complexes were recorded at RT (300 K) and LNT (77 K) using DPPH as the *g*-marker. X-ray diffraction experiments were carried out on XPERT-PRO diffractometer system. Copper Kα_1 line, with wavelength of 1.5406 Å generated with a setting of 30 mA and 40 kV with the electrodes, was used for diffraction. The slit width setting was 91 mm. The diffracting angle (2θ) was scanned from 10.0251 to 79.9251 continuously with a rate of 2°/min. The whole process took place at a temperature of 25 °C. Room temperature magnetic susceptibility measurements were carried out on a modified Gouy-type magnetic balance, Hertz SG8-5HJ. The molar conductivity of the complexes in DMSO solution (10^{-3} M) was measured using a conductometer model 601/602. Voltammetric experiments were performed on a CHI 620C electrochemical analyzer in freshly distilled DMSO solution.

2.2. Preparation of ligands

The ligand $\mathbf{L_2}$ was prepared by employing a two step synthetic method (Scheme 1).

To a solution of 3-hydroxy-4-nitrobenzaldehyde (1.67 g, 0.01 mol) in EtOH was added phenylhydrazine (1.08 g, 0.01 mol) dropwise with constant stirring which immediately precipitated to give a solid red Schiff base ($\mathbf{L_1}$). The product was filtered, washed with hexane and dried *in vacuo*.

To the solution of Schiff base ($\mathbf{L_1}$) (5.14 g, 0.02 mol) in EtOH was added diethyloxalate (1.46 g, 0.01 mol) in 2:1 molar ratio. It was then refluxed for 1 h and cooled to room temperature and then conc. HCl (6 mL) was added dropwise with constant stirring. The resulting mixture was refluxed for 6 h and later the volume of the solution was reduced to half using rotatory evaporator. It was kept aside for some time to yield brownish red solid product, which was filtered and dried *in vacuo*. General formulae of the ligands are shown in Scheme 1.

The spectral data of the ligands are given below:

$\mathbf{L_1}$: red powder, yield 85%, M.F.: $C_{13}H_{11}N_3O_3$, M.Wt: 257.24, M.Pt: 175 °C, Anal. Calcd. (%), C(60.67%), H(4.31%), N(16.37%); found (%) C(60.62%), H(4.29%), N(16.33%); ^{1}H NMR (300 MHz, $CDCl_3$) δ: 10.81 (s, 1H, OH), 6.86–7.52 (m, Ar–H), 8.14 (s, 1H, N=CH), 14.08 (s, 1H, NH); IR(KBr) γ (cm^{-1}): 1593(s) (HC=N), 1620(s) (C–NO_2), 3075(m) (N–H), 3311(s) (O–H), 1327(w) (C–O), 2885(w) (O–H···N), 1421(s) (Ph–C=C), 1533(m) (Ph–C–C), 2981(s) (Ph–C–H).

$\mathbf{L_2}$: brownish red powder, yield 72%, M.F.: $C_{28}H_{20}N_6O_8$, M.Wt: 568.50, M.Pt: 210 °C, Anal. Calcd. (%), C(59.21%), H(3.57%), N(14.76%); found (%) C(59.14%), H(3.52%), N(14.78%); ^{1}H NMR (300 MHz, $CDCl_3$) δ: 10.76 (s, 1H, OH), 6.81–7.58 (m, Ar–H), 8.08 (s, 1H, N=CH); IR(KBr) γ (cm^{-1}): 1658(m) (C=O), 1595(s) (azomethine, HC=N), 1622(s) (C–NO_2), 3309(s) (O–H), 1332(m) (C–O), 2881(w) (O–H···N), 1431(s) (Ph–C=C), 1514(m) (Ph–C–C), 2974(w) (Ph–C–H); UV–Vis (DMF) [nm (frequency, cm^{-1}) (transition)]; 424(23,584) (ILCT), 261(38,314) (ILCT), 248(40,322) (ILCT).

2.3. Synthesis of $[Cu(en)_2]Cl_2$, $[Ni(en)_2]Cl_2$ and $[Zn(en)_2]Cl_2$

These compounds were synthesized by the method reported earlier [8,9].

2.4. Synthesis and characterization of *1*–*3* complexes

To a solution of the ligand ($\mathbf{L_2}$) (0.568 g, 0.001 mol) in EtOH (50 mL) was added $[Cu(en)_2]Cl_2$ (0.254 g, 0.001 mol)/$[Ni(en)_2]Cl_2$ (0.249 g, 0.001 mol)/$[Zn(en)_2]Cl_2$ (0.256 g, 0.001 mol) separately in 1:1 molar ratio in the same solvent. The resulting mixture was magnetically stirred and refluxed for 2 h. The colored precipitate formed was isolated, washed with hexane and dried *in vacuo* (Scheme 1).

$[(L_2)Cu(en)_2]Cl_2$ (1): black powder, yield 65%, M.F.: $[CuC_{32}H_{32}N_{10}O_6]Cl_2$, M.Wt: 787.12, M.Pt: >250 °C, Anal. Calcd. (%), C(48.89%), H(4.13%), N(17.81%), Cu(8.11%); found (%) C(48.81%), H(4.06%), N(17.78%), Cu(8.04%); IR(KBr) γ (cm^{-1}): 1589(s) (azomethine, HC=N), 1323(s) (C–N), 671(s) (CH_2), 1621(w) (C–NO_2), 3311(s) (O–H), 1323(s) (C–O), 3144(s) (–NH_2), 2887(s) (O–H···N), 1448(s) (Ph–C=C), 1533(w) (Ph–C–C), 2966(s) (Ph–C–H); UV–Vis (DMF) [nm (frequency, cm^{-1}) (transition)]; 604(16,556) ($^2B_{1g} \rightarrow {}^2A_{1g}$) (SP), 420(23,809), 262(38,167) (ILCT).

$[(L_2)Ni(en)_2]Cl_2$ (2): light yellow powder, yield 69%, M.F.: $[NiC_{32}H_{32}N_{10}O_6]Cl_2$, M.Wt: 782.26, M.Pt: >250 °C, Anal. Calcd. (%), C(49.19%), H(4.17%), N(17.93%), Ni(7.52%); found (%) C(49.11%), H(4.14%), N(17.87%), Ni(7.46%); IR(KBr) γ (cm^{-1}): 1595(s) (azomethine, HC=N), 1309(w) (C–N), 669(s) (CH_2), 1622(s) (C–NO_2), 3311(b) (O–H), 1327(w) (C–O), 3161(m) (–NH_2), 2881(w) (O–H···N), 1446(s) (Ph–C=C), 1531(m) (Ph–C–C), 2930(w) (Ph–C–H); UV–Vis (DMF) [nm (frequency, cm^{-1}) (transition)]; 698(14,326) ($^1A_{1g} \rightarrow {}^1B_{1g}$) (SP), 610(16,393) ($^1A_{1g} \rightarrow {}^1A_{2g}$) (SP), 421(23,752), 259(38,610) (ILCT), 244(40,983) (ILCT).

$[(L_2)Zn(en)_2]Cl_2$ (3): brownish yellow powder, yield 61%, M.F.: $[ZnC_{32}H_{32}N_{10}O_6]Cl_2$, M.Wt: 788.95, M.Pt: >250 °C, Anal. Calcd. (%), C(48.82%), H(4.11%), N(17.82%), Zn(8.29%); found (%) C(48.71%), H(4.06%), N(17.74%), Zn(8.24%); ^{1}H NMR (300 MHz, $CDCl_3$) δ: 10.78 (s, 1H, OH), 6.97–7.60 (m, Ar–H), 8.10 (s, 1H, N=CH), 3.74–3.81 (m, CH_2), 5.41–5.54 (t, 2H, NH_2); IR(KBr) γ (cm^{-1}): 1600(s) (azomethine, HC=N), 1319(s) (C–N), 671(s) (CH_2),

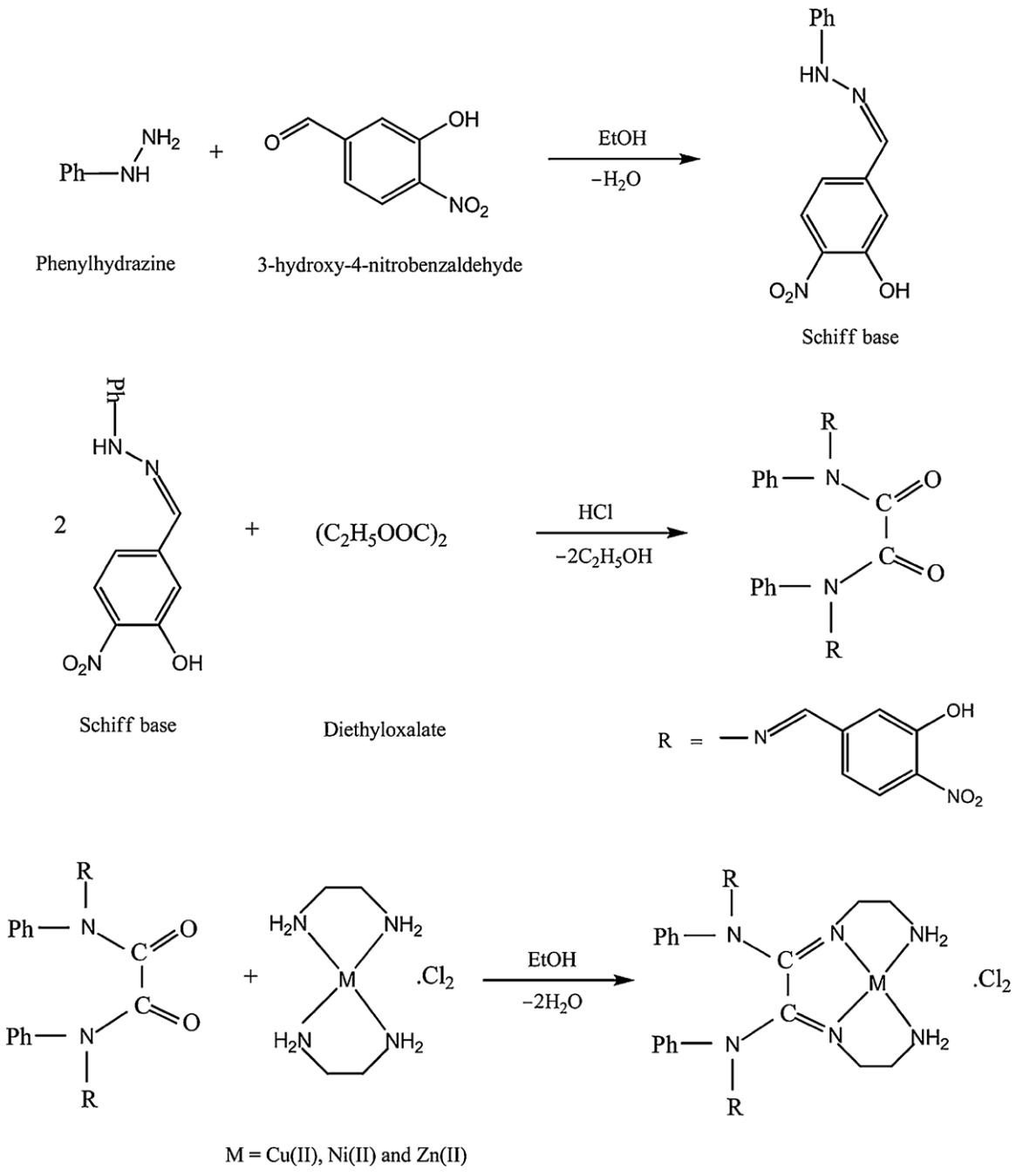

Scheme 1. Synthetic steps for metal complexes.

1643(m) (C–NO_2), 3315(s) (O–H), 1319(s) (C–O), 3165(m) (–NH_2), 2912(b) (O–H···N), 1477(s) (Ph–C=C), 1546(s) (Ph–C–C), 2974(w) (Ph–C–H); UV–Vis (DMF) [nm (frequency, cm^{-1}) (transition)]; 426(23,474), 359(27,855) (ILCT).

2.5. Procedure for DNA-binding and photo-activated cleavage experiments

The DNA-binding and photo-activated cleavage experiments were performed at room temperature. Buffer A [5 mM tris(hydroxymethyl)aminomethane (Tris) hydrochloride, 50 mM NaCl, pH 7.0] was used for absorption titration and viscosity measurements. Buffer B (50 mM Tris–HCl, 18 mM NaCl, pH 7.2) was used for DNA photocleavage experiments.

The absorption titrations of the complex in buffer were performed using a fixed concentration (25 μM) for complex to which increments of the DNA stock solution were added. Metal–DNA solutions were allowed to incubate for 5 min before the absorption spectra were recorded. The intrinsic binding constants K_b, based on the absorption titration, were measured by monitoring the changes of absorption in the MLCT band with increasing concentration of DNA using the following Eq. (1),

$$\frac{[DNA]}{(\varepsilon_a - \varepsilon_f)} = \frac{[DNA]}{(\varepsilon_b - \varepsilon_f)} + \frac{1}{[K_b(\varepsilon_b - \varepsilon_f)]} \quad (1)$$

where [DNA] is the concentration of DNA in base pairs, the apparent absorption coefficients ε_a, ε_f and ε_b correspond to A_{obs}/[complex], extinction coefficient for the free complex and the extinction coefficient of the complex in the totally bound form, respectively. The

data were fitted to Eq. (1), with a slope equal to $1/(\varepsilon_b - \varepsilon_f)$ and y-intercept equal to $1/[K_b(\varepsilon_b - \varepsilon_f)]$ and K_b was obtained from the ratio of the slope to the intercept.

Cyclic voltammetric experiments were performed in a single compartmental cell at 25 °C with DMSO. A three electrode configuration was used, comprised of a glassy carbon as working electrode, Pt wire as auxiliary electrode, and an Ag/AgCl electrode as reference electrode. All the electrochemical measurements were carried out in a 10 mL electrolytic cell using 5 mM Tris–HCl/50 mM NaCl buffer (pH = 7.2) as the supporting electrolyte. Solutions were deoxygenated by purging with N_2 prior to measurements.

The difference between forward and backward peak potentials could provide a rough evaluation of the degree of the reversibility of one electron transfer reaction. The decreased extents of the peak currents observed for all metal(II) complexes upon addition of CT DNA indicated that the complexes interacted with DNA through binding mode. The Nernst equation was used to estimate the ratio of equilibrium constants for the binding of the oxidative and reductive ions to DNA.

$$E_b^\circ - E_f^\circ = 0.0591 \log\left(\frac{K_{red}}{K_{ox}}\right) \quad (2)$$

where E_b° and E_f° are the formal potentials of the bound and free complex forms, K_{red} and K_{ox} are the corresponding binding constants for the binding of reduction and oxidation species to calf thymus (CT-DNA), respectively. The drop of the voltammetry currents in the presence of DNA was attributed to slow diffusion of the metal complex bound to CT DNA indicating the extent of binding affinity of the complex to DNA.

Viscosity measurements were carried out using an Ubbelodhe viscometer, immersed in a thermostatic water-bath that maintained at a constant temperature at 25.0 ± 0.1 °C. The compounds were titrated into the CT-DNA solution (10 μM) present in the viscometer. The flow time of each sample was measured by a digital stopwatch for three times, and an average one was calculated. Data are presented as $(\eta/\eta^0)^{1/3}$ *vs.* binding ratio, where η and η^0 are the viscosity of DNA in the presence and absence of complex, respectively.

Cleavage products were analyzed by agarose gel electrophoresis method [10]. The test samples (25 μg) were added to the pBR322 DNA (0.2 μg). The samples were incubated for 2 h at 37 °C and then 20 μL of DNA sample (mixed with bromophenol blue dye at 1:1 ratio) was loaded carefully into the electrophoresis chamber wells along with standard DNA marker containing TAE buffer (4.84 g Tris base, pH 8.2, 0.5 M EDTA) and finally loaded on agarose gel and passed the constant 60 V of electricity for around 45 min. Then the gel was moved and stained with 10.0 μg/mL ethidium bromide for 10–15 min and the bands were observed under UV light.

To test the presence of reactive oxygen species (ROS) generated during strand scission and possible complex–DNA interaction sites, various reactive oxygen intermediate scavengers and groove binders were added to the reaction mixtures. Due corrections were made for the presence of minor quantity of nicked circular (NC) form in the original SC DNA sample and for the low affinity of EB binding to SC compared to NC and linear forms of DNA. The inhibition reactions were carried out at 365 nm by adding different reagents [DMSO (4 μL), sodium formate (4 μL), KI (4 μL), NaN_3 (200 μM), L-His (100 μM), 20 U/mL SOD, distamycin (5 mM) and EDTA (5 mM)] to DNA prior to the addition of the complex (25 μM).

2.6. Evaluation of antimicrobial activity

Qualitative determination of antimicrobial activity was done using the disc diffusion method. The biological activities of synthesized Schiff base and its metal complexes were studied for their antibacterial and antifungal activities in DMSO solvent against bacterial and fungi species.

Suspensions in sterile peptone water from 24 h cultures of microorganisms were adjusted to 0.5 McFarland. Muller–Hinton petri discs of 90 mm were inoculated using these suspensions. Paper discs (6 mm in diameter) containing 10 μL of the substance to be tested were placed in a circular pattern in each inoculated plate. DMSO impregnated discs were used as negative controls. Toxicity tests of the solvent, DMSO, showed that the concentration used in antibacterial activity assays did not interfere with the growth of the microorganisms.

2.6.1. Determination of MIC

The *in vitro* antimicrobial activity was performed against Gram-positive bacteria: *Salmonella aureus*, *Bacillus subtilis*, Gram-negative bacteria: *Escherichia coli*, *Pseudomonas aeruginosa* and fungal strains: *Rhizoctonia bataticola*, *Rhizopus stolonifer*, *Candida albicans*, *Aspergillus niger*. The standard and test samples were dissolved in DMSO to give a concentration of 100 μg/mL. The minimum inhibitory concentration (MIC) was determined by broth microdilution method [11]. Dilutions of test and standard compounds were prepared in nutrient broth (bacteria) or Sabouraud dextrose broth (fungi) [12]. The samples were incubated at 37 °C for 24 h (bacteria) and at 25 °C for 48 h (fungi), respectively, and the results were recorded in terms of MIC (the lowest concentration of test substance which inhibited the growth of microorganisms).

3. Results and discussion

3.1. Characterization of ligand and its complexes

Several instrumental techniques like IR, UV–vis. spectroscopy, magnetic measurement, ESI-MS, ^{1}H NMR and EPR were used to evaluate the structure of the ligand and its complexes. Microanalytical data were in good agreement with the proposed structure. Experimental section comprises physico-chemical parameters of the ligand and its complexes.

3.1.1. Infrared spectra

The IR spectra of the free ligand and its metal complexes were carried out in 4000–400 cm^{-1} range. The main IR characteristic stretching frequencies of the ligand and its metal complexes along with their proposed assignments are summarized in experimental part.

The IR spectra of the metal complexes were similar to each other, except for some slight shifts and intensity changes of few vibration peaks caused by different metal(II) ions, indicating that the metal complexes had similar structure. However, there were some significant differences between the metal(II) complexes and the free ligand upon chelation, as expected. The coordination mode and sites of ligand to the metal ions were investigated by comparing the IR spectra of the free ligand with its metal complexes.

The ligand **L_2** showed a medium intensity band at 3309 cm^{-1} assigned to –OH group, which remained unaltered suggesting the noninvolvement of the –OH group in coordination with diethyloxalate [13]. The characteristic bands at 3120 and 1475 cm^{-1} due to γ(NH) stretching and bending vibration, were not observed in the IR spectrum of ligand **L_2** indicating the ligand formation through –NH group of phenylhydrazine.

In the complexes, the characteristic band at 1658 cm^{-1} attributed to the disappearance of γ(C=O) [14] whereas the appearance of a new strong band at 1589–1600 cm^{-1} region indicated the condensation of γ(C=O) group with NH_2 group of bis-(ethylenediamine)Cu(II)/Ni(II)/Zn(II) complexes. The formation of γ(C=N) band and the disappearance of the γ(C=O) band in the

complexes commensurated with an effective Schiff's base condensation. A medium intensity band observed at 3144–3165 cm^{-1} in the complexes was assigned to $\gamma(NH_2)$ groups of the other side of bis(ethylenediamine) moiety suggesting 1:1 condensation reaction [15]. In the IR region, the bands appearing at 452, 462 and 447 cm^{-1} were assigned to γ(Cu–N), γ(Ni–N) and γ(Zn– N), respectively, which further confirmed the formation of the complexes [16,11].

3.1.2. Electronic absorption spectra and magnetic moments of metal complexes

Elemental analysis, IR and molar conductivity data were used to prove the stoichiometry and formulation of the complexes. A square-planar geometry was assumed for all the complexes based on their magnetic data and spectral (UV/Vis) studies.

Electronic spectra of ligand and its mononuclear copper(II), nickel(II) and zinc(II) complexes were recorded in the 200–1100 nm range in DMF solution and their corresponding data are given in experimental part. In the electronic spectra of the ligand and its mononuclear metal complexes, the wide range bands were observed due to either the $\pi \rightarrow \pi^*$ and $n \rightarrow \pi^*$ of C=N chromophore or charge-transfer transition arising from π electron interactions between the metal and ligand, which involved either a metal-to-ligand or ligand-to-metal electron transfer [17]. The electronic spectra of the free ligand in DMF showed strong absorption bands in the ultraviolet region (262–424 nm), that could be attributed to the $\pi \rightarrow \pi^*$ and $n \rightarrow \pi^*$ transitions in the benzene ring or azomethine (–C=N) groups for free ligand. The absorption bands between 262 and 424 nm in free ligand changed a bit in intensity and remained slightly changed for metal complexes. The absorption shift and intensity change in the spectra of the metal complexes most likely originated from the metallation, increased the conjugation and delocalization of the whole electronic system and resulted in the energy change of the $\pi \rightarrow \pi^*$ and $n \rightarrow \pi^*$ transitions of the conjugated chromophore [18].

The bands observed between 610 and 698 nm can be attributed to d–d transitions of the metal ions. These values are of particular importance as they are highly dependent on the geometry of the molecule. Thus, the smaller values of the wavelength of the band corresponding to the transitions make a good resemblance between the geometry of the complex and that of square-planar complex.

The electronic spectrum of the complex **1** in DMF revealed a broad band at 604 nm, assigned to $^2B_{1g} \rightarrow {}^2A_{1g}$ transition [19]. It is characteristic of square-planar environment around the Cu(II) ion.

The complex **2** had diamagnetic behaviour and its electronic spectrum showed two peaks at 610 and 698 nm ascribed to $^1A_{1g} \rightarrow {}^1A_{2g}$ and $^1A_{1g} \rightarrow {}^1B_{1g}$ transitions supporting the square-planar geometry around Ni(II) ion [19].

The magnetic susceptibility results of transition metal complexes gave an indication of the geometry of the ligands around the central metal ion. The nickel(II) complex in the present study was diamagnetic and copper(II) complex was paramagnetic. The measured magnetic moment value for complex **1** was 1.74 BM which was very consistent with the expected spin-only magnetic moment *i*.e., $S = 1/2$, a d^9 copper(II) system.

3.1.3. Molar conductance of metal complexes

With a scope to study the electrolytic nature of the mononuclear metal complexes, their molar conductivities were measured in DMSO at 10^{-3} M solution. Molar conductance of the complexes was found in the range 78.32–91.41 $\Omega^{-1}\,cm^2\,mol^{-1}$, suggesting the electrolytic nature of the complexes [20]. The two chloride ions were found to present in the outside of the coordination sphere which was confirmed by Volhard's test.

3.1.4. ^1H NMR spectral studies

^1H NMR spectrum of the ligand and its complex **3** were scanned in the range δ: 0–16 ppm. The ligand $\mathbf{L_1}$ displayed the signals at 14.08 and 10.81 ppm attributed to the N–H of hydrazine and the –OH proton of substituted benzaldehyde [21]. In addition to this, a set of multiplet observed in the range 6.86–7.52 ppm showed the presence of aromatic protons. The ^1H NMR spectrum of the complex **3** displayed signals at 5.41–5.54 and 3.74–3.81 ppm due to $-NH_2$ and $-CH_2$ protons, respectively [22]. These signals further supported the formation of complex by 1:1 condensation reaction.

The comparative study of ^1H NMR data of ligand and its zinc complex revealed the ligational behaviour of the ligand. In the ^1H NMR spectrum of ligand $\mathbf{L_2}$, the signals due to hydrazine N–H proton were absent indicating the condensation between Schiff base ligand $\mathbf{L_1}$ and diethyloxalate. There were no significant changes in the remaining peaks including their intensities.

3.1.5. ESI mass spectral studies

The elemental and analytical data of the copper complex suggested the empirical formula $[CuC_{32}H_{32}N_{10}O_6]Cl_2$, which was further supported by the ESI mass spectrum. The molecular ion peak at 716 *m*/*z* value was observed, corresponding to the mass of the mononuclear complex. The ESI mass spectrum of $\mathbf{L_1}$ Schiff base showed a molecular ion peak at 257 *m*/*z* which is equivalent to its molecular weight and also exhibited two additional peaks at 258 and 259 *m*/*z* corresponding to (M+1) and (M+2) peaks, respectively. The ESI mass spectrum of $\mathbf{L_2}$ exhibited a molecular ion (M^+) peak at 568 *m*/*z* and an additional peak at 569 *m*/*z* corresponding to (M+1) peak. Apart from these, the spectrum showed few peaks at 166, 255, 256, 402, 403, 236, 333 and 334 *m*/*z* which are due to various fragments of $\mathbf{L_2}$. By comparing all the analytical and spectral data of nickel and zinc complexes, it is evident that these are monomeric complexes.

3.1.6. EPR studies

The X-band EPR spectrum of copper(II) complex was recorded in the solid state at room temperature and also in DMSO at 77 K using DPPH as the '*g*' marker (Fig. 1). The solution spectrum of the complex possessed well-resolved $g_\parallel$ and a broad $g_\perp$ region. The four peaks in the spectrum were evidently due to the coupling of the electron spin of the ^{63}Cu nucleus ($I = 3/2$). The peaks were broad and had the appearance of ill-resolved triplets. The breadth and triplet appearance could be attributed to hyperfine splitting by the nitrogen atom ($I = 1$) of the ligand. The triplet appearance might be added as an evidence for nitrogen coordination. Based on the observation, a distorted square-planar geometry was proposed for the complex. Various Hamiltonian parameters had been calculated for this complex ($g_\parallel = 2.22, g_\perp = 2.06$). Here for the complex **1**, $g_\parallel > g_\perp$ suggested a square-planar geometry [23]. For the present copper complex, g_{av} was calculated using the equation, $g_{av} = 1/3(g_\parallel + 2g_\perp)$ and it was found to be 2.11. The spectrum of the complex had four hyperfine lines in both parallel and perpendicular regions. $A_\parallel$ and $A_\perp$ were calculated to be 200×10^{-4} and $90 \times 10^{-4}\,cm^{-1}$, respectively. A_{av} was calculated using the formula $A_{av} = 1/3\,(A_\parallel + 2A_\perp)$ and it was $126.66 \times 10^{-4}\,cm^{-1}$. It has been reported that $g_\parallel$ value of copper(II) complex can be used as a measure of the covalent character of the metal–ligand bond. If the value is more than 2.3, the metal–ligand bond is essentially an ionic and if the value is less than 2.3, it is an indicative of covalent character [24]. Here the $g_\parallel$ value, 2.22 confirmed the covalent nature of copper complex in conformity with the presence of copper–nitrogen bonds in these complexes. Moreover, the trend $g_\parallel > g_\perp > g_e$ observed for the complex indicated the unpaired electron in the d_{x2-y2} orbital of the Cu(II) ion, a characteristic of axially symmetric complex [25]. The empirical ratio $g_\parallel/A_\parallel$ was frequently used to evaluate distortions in

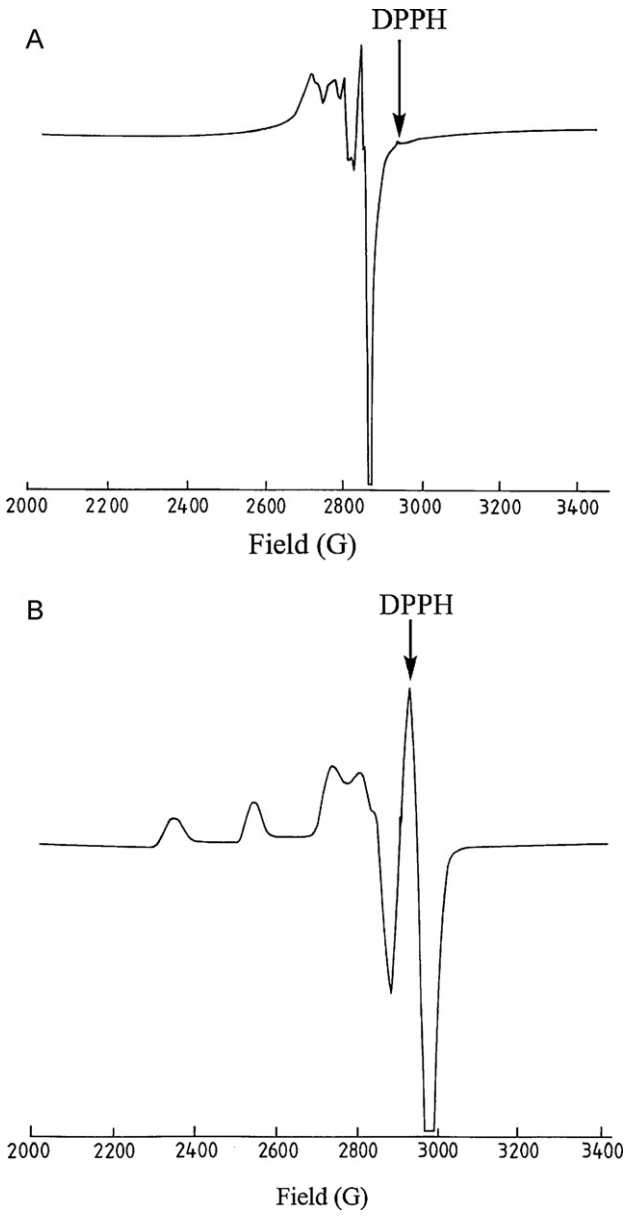

Fig. 1. EPR spectra of complex **1** at (A) RT (300 K) and (B) LNT (77 K).

tetra coordinated copper(II) complexes [26]. The ratio close to 100, indicated a roughly square-planar structure around the copper(II) ion [27] and the values from 170 to 250 indicated a distorted tetrahedral geometry. Here, the value of the $g_{\parallel}/A_{\parallel}$ ratio for complex **1** (1 1 1) nearly indicated the square-planar environment around the Cu(II) ion with small distortions.

In axial symmetry, the *g*-values were related to the *G*-factor by the expression, $G = (g_{\parallel} - 2)/(g_{\perp} - 2)$, which measured the exchange interaction between copper centers in the solid. According to Hathaway and Billing [28], if the value of *G* is greater than 4, the exchange interaction between copper(II) centers in the solid state is negligible, whereas when it is less than 4, a considerable exchange interaction exists in the solid complex. The geometric parameter *G* for complex **1** was 3.79 which is less than 4, supporting that a less exchange interaction is present in the copper complex.

The parameters $g_{\parallel}$, $g_{\perp}$, $A_{\parallel}$ and $A_{\perp}$ of complex and the energies of the d–d transitions were used to calculate the orbital reduction parameters ($K_{\parallel}$, $K_{\perp}$) and the bonding parameters (α^2 and β^2). The factors α^2 and β^2 are usually taken as measure of covalency which

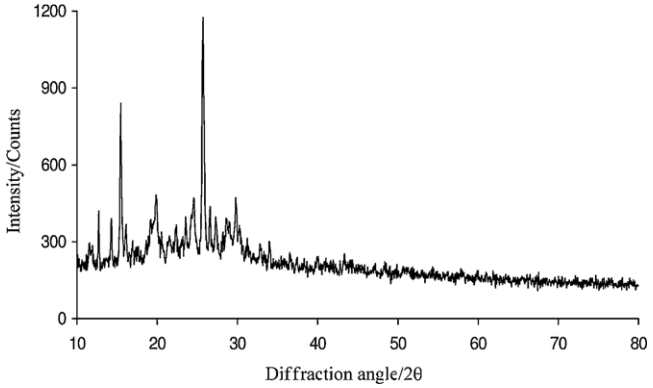

Fig. 2. Powder X-ray diffraction pattern of complex **2**.

is evaluated by the expression:

$$\alpha^2 = -\left(\frac{A_{\parallel}}{0.036}\right) + (g_{\parallel} - 2.0027) + \left(\frac{3}{7}\right)(g_{\perp} - 2.0027) + 0.04$$

$$\beta^2 = (g_{\parallel} - 2.0027)\frac{E}{-8\lambda\alpha^2}$$

where $\lambda = -828\ \mathrm{cm}^{-1}$ for the free copper ion and *E* is the electronic transition energy. The covalency of the in-plane σ-bonding, $\alpha^2 = 1$ indicates the complete ionic character, whereas $\alpha^2 = 0.5$ denotes 100% covalent bonding. The α^2 value for the copper complex **1** was 0.83, supporting the covalent nature. The β^2 parameter gave an indication of the covalency of the in-plane π-bonding. The smaller the β^2 (0.64), the larger is the covalency of the bonding. For the copper(II) complex, the low value of β^2 compared to α^2 indicated that the in-plane π-bonding was more covalent than the in-plane σ-bonding. Hathaway [29] pointed out that for pure σ-bonding, $K_{\parallel} \approx K_{\perp} = 0.77$ and for in-plane π-bonding $K_{\parallel} < K_{\perp}$, while for out-of-plane π-bonding, $K_{\perp} < K_{\parallel}$. The following simplified expressions were used to calculate $K_{\parallel}$ and $K_{\perp}$:

$$K_{\parallel} = (g_{\parallel} - 2.0027)\ \text{d–d transition}/8\lambda_0$$
$$K_{\perp} = (g_{\perp} - 2.0027)\ \text{d–d transition}/2\lambda_0$$

The observed $K_{\parallel}$ (0.5431) < $K_{\perp}$ (0.5728) relation indicated the presence of significant in-plane π-bonding. Thus, the EPR study of the copper(II) complex has provided supportive evidence to the conclusion obtained on the basis of electronic spectrum and magnetic moment value.

3.1.7. X-ray powder diffraction

Single crystal X-ray crystallographic investigation is the most precise source of information regarding the structure of the complexes, but the difficulty of obtaining crystalline complexes in proper symmetric form has rendered the powder X-ray diffraction method for such study. Powder XRD pattern of the Schiff base complexes were recorded over the $2\theta = 0$–80 range and complex **2** are shown in Fig. 2. The trend of the curves decreases from maximum to minimum intensity indicating that these complexes are amorphous in nature in the present metal–ligand formation.

The diffractogram of **2** consists of 10 reflections with maxima at $2\theta = 25.695^{\circ}$ corresponding to value of $d = 3.4641$ Å (Table 1). The main peaks of **2** had been indexed using computer software by trial and error method, keeping in mind characteristics of various symmetry systems until good fit could be obtained between observed and calculated 2θ and $\sin^2\theta$ values. The method also yielded *hkl* (Miller indices) values. The relative intensities corresponding to prominent peaks had also been measured. The X-ray data revealed

Table 1
X-ray diffraction data of complex **2**.

2θ (Cal.)	2θ (Obser.)	Sin² θ (Cal.)	Sin² θ (Obser.)	d (Å) (Cal.)	d (Å) (Obser.)	h k l	Intensity (%)
15.445	16.797	0.0180	0.0188	5.7321	5.6053	1 1 0	64.76
16.079	16.332	0.0195	0.0201	5.5076	5.4230	0 0 1	16.28
19.675	19.796	0.0291	0.0295	4.5084	4.4813	1 1 1	20.62
25.695	25.853	0.0494	0.0500	3.4641	3.4435	0 2 0	100.00
28.805	28.721	0.0618	0.0615	3.0968	3.1057	3 1 1	14.06
29.861	29.472	0.0663	0.0647	2.9896	3.0283	2 0 1	14.96
32.883	32.978	0.0801	0.0805	2.7237	2.7139	1 1 2	8.08
37.366	37.249	0.1026	0.1019	2.4066	2.4119	4 0 0	4.36
39.905	39.600	0.1164	0.1147	2.2592	2.2740	2 2 1	4.58
50.994	50.444	0.1852	0.1815	1.7894	1.8076	0 0 3	4.30

that the complex **2** had crystallized in the face-centered monoclinic system. The azomethine of **2** exhibited the main reflection at $2\theta = 25.695^{\circ}$ (d spacing 3.4641 Å).

3.1.8. Electrochemistry

Electrochemistry of these newly synthesized Schiff base metal complexes **1**–**3** was studied by cyclic voltammetry in the scan rate of 0.080 V s^{-1} in DMSO solution containing 0.1 M TBAP supporting electrolyte and redox potentials were expressed with reference to Ag/AgCl. All the measurements were carried out in the potential range +1.5 to −1.5 V and are listed in Table 2.

The electrochemical potentials of these complexes were characterized by well-defined waves in cathodic and anodic regions. Since the ligands used in this work were not reversibly oxidized or reduced in the applied potential range, the redox processes were assigned to the metal centers only.

The ligand showed an irreversible oxidation at 0.056 V (Epa) and an irreversible reduction at −1.008 V (Epc) *vs.* Ag/AgCl in the scan rate of 0.08 V s^{-1}. Complex **2** exhibited one anodic wave at Epa = −0.081 V with corresponding cathodic wave at Epc = −0.808 V. The processes of **2** were quasi-reversible with the corresponding anodic–cathodic peak separations (ΔE) for the couple Ni(II)/Ni(I) and half-wave potentials ($E_{1/2}$) were calculated as the average of the anodic and cathodic peak potentials of the processes, which are given in Table 2.

Attempting to elucidate correlations between structural and redox characteristics, the redox properties of the Cu(II)/Cu(I) couple have been extensively studied and a number of factors which affect Cu(II)/Cu(I) redox potential have already been identified. The copper(II) complex **1** showed a quasi-reversible Cu(II)/Cu(I) couple at formal potential $E_{1/2} = -0.672$ V. This couple can be attributed to the reduction occurring at the Cu(II) center in the imine nitrogen site of Schiff base ligand and the strong σ-donor tendency of the ethylenediamine moiety [30].

For complex **1**, a wave (Epc = −0.946 V) corresponding to the reduction of Cu(II) to Cu(I) was obtained. During the reverse scan, the oxidation of Cu(I) to Cu(II) occurred at the potential of Epa = −0.399 V. The values of the limiting peak-to-peak separation (ΔEp = −0.547 V) revealed that this process could be quasi-reversible. Therefore, it was inferred that both the Cu(II) complexes underwent reduction to their respective Cu(I) complexes which subsequently underwent disproportionation to Cu(0) and Cu(II). The oxidative responses around 0.596 V might be due to the Cu(II)/Cu(III) couple.

The cyclic voltammogram for **3** recorded at a scan rate of 0.080 V s^{-1} displayed a reduction peak at Epc = −0.781 V with no oxidation peak. The reduction wave could be assigned to the reduction process of Zn(II) to Zn(I).

It was also observed that the ligand moiety had a significant effect on $E_{1/2}$ for all the complexes; electronwithdrawing groups stabilized the metal(II) in the complexes while the electron-donating group favored oxidation to metal(III). It was probable, because the electron-withdrawing anion made the complex more positively charged and favored the reduction of metal ion. Similarly the electron-donating groups made the complexes less positively charged.

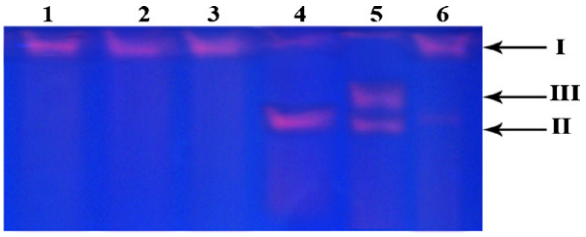

Fig. 3. Cleavage of pBR322 DNA by complex **1** in the presence of peroxide. DNA (0.2 μg) incubated with **1** for 90 min in Tris buffer (pH 7.2). Lane 1: DNA control; lane 2: DNA + **1** (25 μM) alone; lane 3: DNA + peroxide (200 μM) alone; lane 4: DNA + **1** (25 μM) + peroxide (300 μM); lane 5: DNA + **1** (25 μM) + peroxide (400 μM); lane 6: DNA + **1** (25 μM) + peroxide (400 μM) + ethanol (15 μM).

3.2. Biological evaluation

3.2.1. DNA unwinding studies

3.2.1.1. Hydrolytic cleavage of pBR322 DNA. Copper(II) complexes are able to cleave DNA through both oxidative and hydrolytic processes. The possibility of a hydrolytic mechanism for the DNA cleavage by the complex **1** must be taken into account.

Fig. 3 shows the electrophoretic pattern of plasmid DNA treated with complex **1**. Control experiments suggested that untreated DNA and DNA incubated with either complex or peroxide did not show any significant DNA cleavage (lanes 1–3). However, in the presence of peroxide, complex **1** was found to exhibit nuclease activity. In the presence of 25 μM of complex **1** and 300 μM of peroxide, the plasmid DNA was nicked as evident from the formation of Form II and the disappearance of the supercoiled form in the electrophoretic experiment (lane 4). At the same concentration of the complex and a slightly higher concentration of peroxide (400 μM), the cleavage was found to be much efficient as seen from the formation of linear form (Form III) in lane 5. Thus, the nuclease activity of the complex **1** could be ascribed to the cooperative effect between Cu(II) ion and $\mathbf{L_2}$ ligand. Nuclease activity exhibited by certain copper(II) complex in the presence of hydrogen peroxide indicated the participation of hydroxyl radical in DNA cleavage. The addition of ethanol to the reaction mixture before electrophoresis was found to suppress the DNA cleaving ability of the complexes (lane 6). It conclusively showed the involvement of the hydroxyl radical in the observed nuclease activity of complex **1** in the presence of peroxide.

3.2.1.2. Photo-activated cleavage of pBR322 DNA by complexes. The cleavage of plasmid DNA could be monitored by agarose-gel electrophoresis. When circular plasmid DNA was subjected to electrophoresis, relatively fast migration was generally observed for the intact supercoiled Form I. When scission occurred on one strand

Table 2
Redox couples of the complexes, their potentials and the shift of the potentials in the absence and presence of CT-DNA.

Complex	Redox couple	Ipc (A) × 10^{-5}		Epc (V)		$E_{1/2}$ (V)		ΔEp (V)		K_{ox}/K_{red}
		Free	Bound	Free	Bound	Free	Bound	Free	Bound	
1	Cu(II)/Cu(I)	2.43	1.88	−0.946	−0.927	−0.672	−0.666	0.547	0.522	2.09
	Cu(I)/Cu(0)	4.05	3.30	−1.215	−1.193	–	–	–	–	2.35
2	Ni(II)/Ni(I)	4.28	4.07	−0.808	−0.791	−0.444	−0.468	0.727	0.645	1.93
3	Zn(II)/Zn(I)	1.17	0.99	−0.781	−0.832	–	–	–	–	0.13

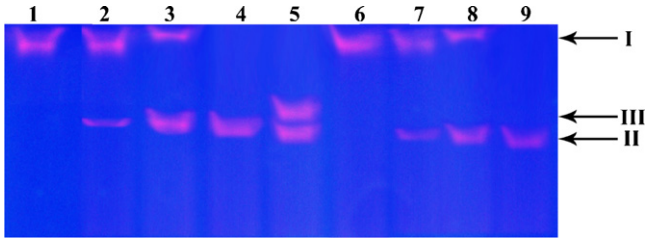

Fig. 4. Gel electrophoresis diagram showing the cleavage of pBR322 DNA (0.2 μg) at different complex concentrations in Tris–HCl/NaCl buffer (pH = 7.2) at 37 °C on irradiation with UV light for 1.5 h. Photograph showing the effects of transition metal complexes on DNA, lane 1: DNA control; lanes 2–5: DNA + **1** (10, 20, 30, 40 μM), respectively; lanes 6–9: DNA + **2** (10, 20, 30, 40 μM), respectively.

(nicking), the supercoil relaxed to generate a slower-moving, open circular Form II. When both strands were cleaved, a linear Form III was generated, migrating between Form I and Form II DNA [31].

In Fig. 4, the gel electrophoresis pattern of pBR322 DNA is shown after incubation with complex **1** or **2** and irradiation at 365 nm. No DNA cleavage was observed for negative control (lane 1). With increasing concentration of the copper(II) complex **1** (lanes 2–5) and nickel(II) complex **2** (lanes 6–9), the amount of Form I of pBR322 DNA diminished gradually, whereas Form II increased and Form III was also produced. Whereas for complex **1**, at the concentration of 40 μM, significant amounts of linear DNA (Form III) were visible, which indicated that, under comparable experimental conditions, complex **1** exhibited more effective DNA cleavage activity than complex **2**. These different cleavage efficiencies paralleled the observed DNA-binding affinities of the two complexes, as was reported in other cases [32].

The involvement of reactive oxygen species (ROS) such as hydroxyl, superoxide, singlet oxygen-like species and hydrogen peroxide in the nuclease mechanism was determined by monitoring the quenching of the DNA cleavage in the presence of ROS scavengers which are shown in Fig. 5. Control experiments suggested that untreated DNA did not show any cleavage in the dark and even upon irradiation by light. In order to observe the reactive species that were responsible for the DNA damage, we investigated the DNA cleavage in the presence of hydroxyl radical

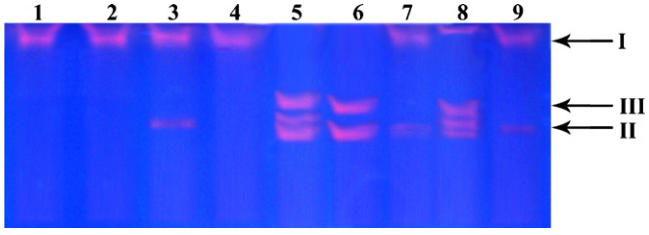

Fig. 5. Gel electrophoresis diagram showing the cleavage of SC pBR322 DNA (0.2 μg) by the complex **1** (25 μM) in Tris–HCl/NaCl buffer (50 mM, pH 7.2) in the presence of various reagents on photo-irradiation with UV light for 1 h: lane 1: DNA control; lane 2: DNA + DMSO (4 μL) + **1**; lane 3: DNA + sodium formate (4 μL) + **1**; lane 4: DNA + KI (4 μL) + **1**; lane 5: DNA + NaN_3 (200 μM) + **1**; lane 6: DNA + L-His (100 μM) + **1**; lane 7: DNA + 20 U/mL SOD + **1**; lane 8: DNA + distamycin (5 mM) + **1**; lane 9: DNA + EDTA (5 mM) + **1**.

scavengers (DMSO, sodium formate, KI), singlet oxygen quenchers (L-histidine, NaN_3), superoxide scavenger (superoxide dismutase enzyme SOD), minor groove binder (distamycin) and chelating agent (EDTA) under our experimental conditions.

The hydroxyl radical scavengers DMSO, sodium formate and KI (lanes 2–4) diminished the DNA breakdown of complex **1**, which indicated that the hydroxyl radical was participated in the oxidative cleavage. Sodium azide and L-histidine (lanes 5 and 6) had no significant effect on the DNA cleavage. This fact ruled out the involvement of the participation of $^1O_2$ or singlet oxygen-like entities in the reaction. The significant reduction in the ability of complex **1** to cleave DNA in the presence of the superoxide- dismutase enzyme (lane 7) suggested that O_2^- was one of the reactive species that actually broke the DNA. No apparent inhibition of DNA damage was observed in the presence of the minor groove binder distamycin (lane 8), suggesting the lack of interaction of complex **1** through the DNA minor groove. The EDTA, a copper(II)-specific chelating agent that strongly bound to copper(II) forming a stable complex, could efficiently inhibit DNA cleavage, indicating copper(II) complexes played the key role in the cleavage.

3.2.1.3. Viscosity studies. To further clarify the binding mode between the complexes and DNA, viscosity measurements were carried out on CT-DNA by varying the concentration of the complexes. Intercalation of the complex to DNA is known to cause a significant increase in the viscosity of DNA solution due to an increase in the separation of the base pairs at the intercalation site and, hence, an increase in the overall DNA molecular length. In contrast, a partial and/or non-classical intercalation could bind (or kink) the DNA helix and concomitantly reduce its effective length and viscosity.

The effect of each investigated complex on the viscosity of CT-DNA solution was studied in order to assess the binding mode and strength of these complexes with DNA. Representative plots of η/η^0 *vs.* [complex]/[DNA] are shown in Fig. 6 for the investigated complexes. With an increasing amount of complex **3**, the relative viscosity of DNA decreased and then increased gradually while the increasing amount of complex **1** and **2** further reduced the effective length of DNA supporting that both the complex **1** and **2** bound through partial non classical intercalation mode but with different affinity. However, complex **1** showed strong binding in comparison to complex **3** presumably due to electrostatic interaction with DNA [33]. The effect on the CT-DNA shown in Fig. 6 revealed that the relative viscosity of DNA increased steadily in the following order, **1** > **2** > **3** with an increasing amount of the above compounds.

Several factors which include the shape and hydrophobicity of the complex as well as extension of planarity and the presence of additional donor functionalities on the ligand have been cited to be an importance in rendering these complexes to be strong intercalative, electrostatic binding agents. It should be noted here that each ethylenediamine-based complex investigated in the present study also exhibited spectral, electrochemical and viscosity changes in the presence of DNA that were analogous to those exhibited by the complexes mentioned above. The increased degree of viscosity may depend on the affinity of the compounds to DNA, which is also consistent with our foregoing hypothesis.

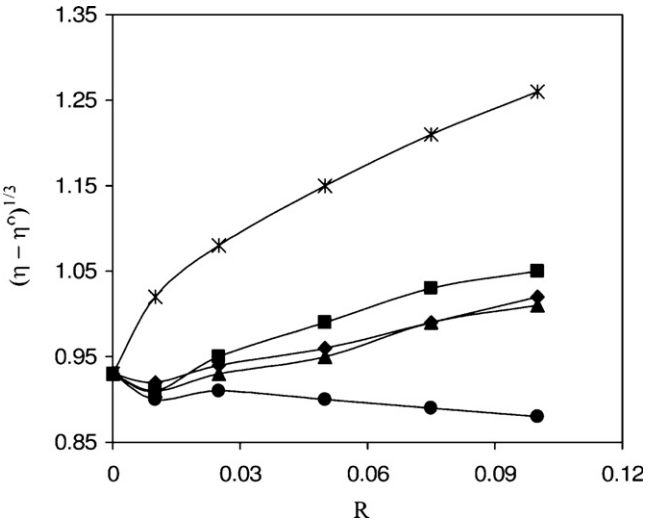

Fig. 6. Effect of increasing amount of EB (*), $[Ru(bpy)_3]^{2+}$ (●) and in presence of increasing concentration of complexes of 1 (■), 2 (♦) and 3 (▲) on the relative viscosity of CT-DNA at 30 °C. [DNA] = 10 μM, R = [complex]/[DNA] or [EB]/[DNA].

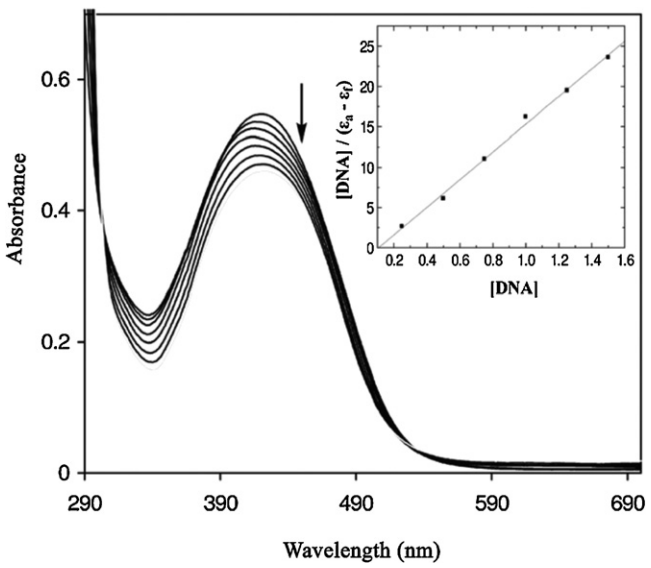

Fig. 7. Absorption spectra of complex **1** in presence of DNA in Tris–HCl buffer upon addition of CT DNA. [complex] = 25 μM. Arrow shows the absorbance changing upon the increase of DNA concentration.

3.2.2. Interactions with DNA

The interactions of metal complexes with DNA have been the subject of interest for the development of effective chemotherapeutic agents. Transition metal centers are particularly attractive moieties for such research since they exhibit well-defined coordination geometries and also possess distinctive electrochemical or photophysical properties, thus enhancing the functionality of the binding agent. The interaction of the complexes with CT DNA has been studied with UV spectroscopy and CV in order to investigate the possible binding mode to CT DNA and to calculate the binding constants (K_b) [34].

3.2.2.1. Absorption spectral features in DNA binding. The absorption spectra are the most common means to examine the interaction between metal complex and DNA. In general, the absorption spectra of metal complexes bound to DNA through intercalation exhibit significant hypochromism and red shift due to the strong π–π stacking interaction between the aromatic chromophore ligand of metal complex and the base pairs of DNA [35].

When the $\mathbf{L_2}$ ligand of the ethylenediamine based metal(II) complexes intercalated into the base pairs of DNA, its π* orbital was coupled with the π orbital of DNA base-pairs to give rise to the decrease in the π–π* transition energies. As a result, the λ_{max} of the intra ligand transition of the $\mathbf{L_2}$ ligand was shifted to the longer wavelength (red shift). On the other hand, the coupled π* orbital of the $\mathbf{L_2}$ ligand of the ethylenediamine based metal(II) complexes were also partially occupied by electrons due to overlapping with the π orbital of the DNA base pairs (effect of charge transfer) to decrease the transition probabilities. Consequently, the transition intensity was weakened, resulting in hypochromic effect [36]. The hypochromic effect, characteristic of intercalation has been usually attributed to the interaction between the electronic states of the compound chromophores and those of the DNA bases [37].

The binding of complexes **1**–**3** to DNA helix have been characterized through absorption spectral titrations, by following changes in absorbance and shift in wavelength. In Fig. 7, the absorption spectra of the metal(II) complex **1** (at a constant concentration) were shown in the absence and presence of CT-DNA. The absorption spectra of the metal(II) complex **2** (at a constant concentration) in the absence and presence of CT-DNA were included in the supplementary material (Fig. S1). In the UV region, the **1**–**3** complexes exhibited two intense absorption bands: one at 400–425 nm which was attributed to the ligand-to-metal charge transfer transition (LMCT), and the other in the region 240–262 nm which was assigned to the intraligand (π–π*) transition of the aromatic chromophore. With increasing CT DNA, the absorption bands of the complexes were affected, resulting in the obvious tendency of hypochromism and slight shifts to longer wavelengths, which indicated that the four N-containing **1**–**3** complexes could interact with CT DNA. The results showed that upon addition of DNA to complex **1**, more binding activity was observed than that of **2** and **3**. The hypochromism observed were 13.60% for **1**, 12.31% for **2** and 14.67% for **3**, respectively. The $[DNA]/(\varepsilon_a - \varepsilon_f)$ ratio was plotted against [DNA] and intrinsic constants K_b were obtained from the ratio of the slope to the intercept. The K_b values obtained for complexes **1**, **2** and **3** were $9.37 \times 10^5\ M^{-1}$, $3.16 \times 10^5\ M^{-1}$ and $4.59 \times 10^5\ M^{-1}$, respectively. The significant difference in DNA-binding affinity of the three metal(II) complexes could be understood as a result of the fact that the complex with higher numbers of metal(II) chelates showed stronger binding affinity with DNA. Our results are consistent with earlier reports on preferential binding to CT DNA in the metal complexes [38].

3.2.2.2. Effect of electrode potential on metal complex and CT-DNA interactions. The electrochemical investigations of metal–DNA interactions could also provide a useful supplement to spectroscopic methods and yield information about interactions (electrostatic or intercalative) with both the reduced and oxidized form of the metal. The difference between voltammetric responses of **1** in the absence and presence of CT-DNA are depicted in Fig. 8 whereas the difference between voltammetric responses of **3** in the absence and presence of CT-DNA is included in the supplementary file (Fig. S2). The significant shift in peak potentials and current ratios of **1**–**3** were observed upon addition of CT-DNA. The summary of voltammetric results for **1**–**3** in the absence and presence of CT-DNA is given in Table 2. No new redox peaks had appeared after the addition of CT DNA to each complex, but the current intensity decreased significantly, suggesting the existence of an interaction between each complex and CT DNA, explained in terms of an equilibrium mixture of free and DNA-bound complex on the electrode surface [39].

The electrochemical investigations of metal–DNA interactions are a useful complement to spectroscopic methods and can provide information about interactions with both the reduced and oxidized

Table 3
Antimicrobial activity, expressed in MIC (μg/mL), of complexes and ligands on the positive and negative bacteria and fungal strains.

Complex	Antibacterial activity				Antifungal activity			
	S. aureus	*B. subtilis*	*E. coli*	*P. aeruginosa*	*A. niger*	*R. stolonifer*	*C. albicans*	*R. bataicola*
L_1	19.27	19.34	17.08	18.21	21.06	18.32	17.95	18.28
L_2	18.96	17.34	15.24	16.57	16.27	18.17	16.22	18.31
1	5.37	6.48	4.41	5.58	7.19	5.26	4.97	6.23
2	7.64	8.71	7.82	6.18	7.28	5.37	6.37	8.46
3	6.38	5.72	6.37	5.27	7.11	6.31	5.14	7.56
Streptomycin	1.98	2.32	1.04	1.16	–	–	–	–
Nystatin	–	–	–	–	1.82	2.35	2.18	1.96

form of the metal. The electrochemical potential of a small molecule will shift positively when it intercalates into DNA double helix, and, if it is bound to DNA by electrostatic interaction, the potential will shift to a negative direction. Additionally, if more potentials than one present such a shift, a positive shift of Epa and a negative shift of Epc may imply that the molecule can bind to DNA by both intercalation and electrostatic interaction [40].

Complexes **1** and **2** exhibited the same electrochemical behaviour upon addition of CT DNA with a positive shift for the cathodic potential Epc (ΔEpc = +0.019 V and +0.017 V for **1** and **2**, respectively) (Table 2) and the anodic potential Epa shifting to negative values (ΔEpa = (−0.006 V and −0.065 V for **1** and **2**, respectively). These shifts showed that **1** and **2** could bind to DNA by both intercalative and electrostatic interaction [40,41]. On the other hand, a negative shift of the cathodic potentials for **3** (ΔEpc = −0.051 V) and no anodic potential was observed. Thus, the existence of electrostatic interaction between **3** and CT DNA bases may be suggested [40]. The presence of DNA in the solution at the same concentration of three complexes caused a considerable decrease in the voltammetric current. The drop of the voltammetric currents in the presence of CT DNA could be attributed to diffusion of the metal complex bound to the large, slowly diffusing DNA molecule. The decrease extents of the peak currents observed for three complexes upon addition of CT DNA indicated that the DNA binding affinity increased in the order: **3** < **2** < **1**. The results paralleled to the above spectroscopic and viscosity data of three complexes in the presence of DNA.

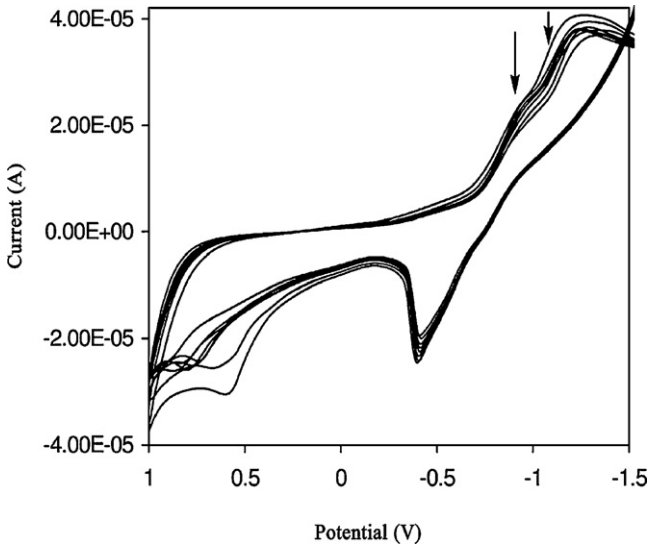

Fig. 8. Cyclic voltammograms in DMSO:buffer [mixture 50 mM Tris–HCl/NaCl buffer (pH, 7.0)] (1:2) solution of complex **1** carried out at scan rate = 0.08 V s^{-1} with incremental addition of CT DNA. 0.1 M n-Bu_4NClO_4 as supporting electrolyte and the arrow mark indicates the current changes upon increasing DNA concentration.

3.2.3. Antimicrobial studies

From the *in vitro* antimicrobial screening results (Table 3 and supplementary Fig. S3), it was observed that the ligand was moderately active against the bacteria and fungi used. All the complexes exhibited higher activity in comparison with the ligand against both the bacteria and fungi. The remarkable activity of the Schiff base metal complexes may be arise from the hydroxyl groups, which may play an important role in the antibacterial activity, as well as the presence of imine groups which import in elucidating the mechanism of transformation reaction in biological systems. Among the complexes, the complex **1** exhibited better activity than **2** and **3** against all the microorganisms used. On the other hand, the electron-withdrawing substituent such as nitro group on the benzene ring exhibited a comparable growth-inhibitory activity against microorganisms. Our results showed that the tested compounds exhibited a specific antimicrobial activity, both concerning the microbial spectrum and the MIC value.

The comparative screening of the antimicrobial properties of complexes **1**–**3** exhibited an improved microbicidal effect as compared with the ligands. In case of *E. coli* compound **1** emerged as effective antibacterial agent having MIC value 4.41 μg/mL. In case of *P. aeruginosa*, compounds **1** and **3** had shown good antibacterial capability at MIC values 5.58 μg/mL and 5.27 μg/mL, respectively, and in case of *B. subtilis* compound **3** had shown good antibacterial capability at a MIC value 5.72 μg/mL. For antifungal activity against *C. albicans*, compounds **1** and **3** showed marked antifungal potential having MIC values 4.97 μg/mL and 5.14 μg/mL, respectively, as compared to other synthesized complexes. In case of *R. stolonifer*, compounds **1** and **2** were found to be most active with MIC values 5.26 μg/mL and 5.37 μg/mL, respectively. However, it was to be mentioned that zinc(II) complex exhibited good antimicrobial activity, followed by copper species. The reason for this higher antimicrobial efficacy could be related to the inhibition by several structural enzymes, which play a key role in vital metabolic pathways of the microorganisms. It was demonstrated that the above metal complexes showed a higher effect on *E. coli* and *P. aeruginosa* than on *S. aureus* and this difference could be due to the Gram-status. It is known that the membrane of Gram-negative bacteria is surrounded by an outer membrane containing lipopolysaccharides. The newly synthesized Schiff bases seem to be able to combine with the lipophilic layer in order to enhance the membrane permeability of the Gram-negative bacteria. The lipid membrane surrounding the cell favors the passage of only lipid soluble materials; thus the lipophilicity is an important factor that controls the antimicrobial activity. Moreover, the increase in lipophilicity enhances the penetration of Schiff bases into the lipid membranes and thus restricts further growth of the organism. This could be explained by the charge transfer interaction between the Schiff base molecules and the lipopolysaccharide molecules which lead to the loss of permeability barrier activity of the membrane.

Such an enhanced activity of the complexes can be explained on the basis of Overtone's concept and Tweedy's chelation theory [42]. According to Overtone's concept of cell permeability, the lipid

membrane that surrounds the cell favors the passage of only lipid soluble materials due to which liposolubility is an important factor that controls antimicrobial activity. On chelation, the polarity of the metal ion is reduced to a greater extent due to the overlap of the ligand orbital and partial sharing of the positive charge of the metal ion with donor groups. Further, it increases the delocalization of π-electrons over the whole chelate ring and enhances the lipophilicity of the complexes. This increased lipophilicity enhances the penetration of the complexes into lipid membranes and blocking of metal binding sites on the enzymes of the microorganisms. These complexes also disturb the respiration process of the cell and thus block the synthesis of the proteins that restricts further growth of the organism. The variation in the effectiveness of the different compounds against different organisms depends on the impermeability of the cells of microbes or difference in ribosome of the microbial cells.

4. Conclusion

The synthesis and characterization of three new metal(II) complexes of Cu(II), Ni(II) and Zn(II) have been realized with physicochemical and spectroscopic methods. Each metal is four-coordinate and hence, the geometry can be described as square-planar. In the cyclic voltammograms of the complexes recorded in DMSO, the irreversible or, in most cases, quasi-reversible waves attributed to redox couples, characteristic for each metal complex, have been recorded at potentials expected for the central metal. The study of the interaction of complexes with CT DNA has been performed with UV spectroscopy and cyclic voltammetry. It reveals the ability of synthesized metal complexes **1**–**3** to bind to DNA. The binding strength of the complexes with CT DNA calculated with UV spectroscopic titrations have shown that complex **1** exhibits the highest K_b value among the compounds examined. Cyclic voltammetric study proposes both intercalative and electrostatic interaction as the most possible binding mode to DNA. The better binding properties of the complexes should be attributed to the good coplanarity of the ligand after coordination with metal ions. Meanwhile, nature of the central metal ions also affects the intercalative ability. These results indicate that DNA might also serve as the primary target of these compounds; in addition, they should have many potential practical applications, just like the promising therapeutic drug candidates. All the complexes can effectively cleave plasmid DNA without addition of external agents. DNA cleavage mechanism studies show that the complexes examined here may be capable of promoting DNA cleavage through both oxidative and hydrolytic DNA damage pathways. They display higher nuclease activity of the Cu(II) complex than other complexes and hence, the cooperative interaction of metal ions is a favored factor to cleave DNA.

We have evaluated *in vitro* antibacterial and antifungal activities for our newly synthesized Schiff base and its mononuclear copper(II), nickel(II) and zinc(II) complexes. The results obtained from this research demonstrate that newly synthesized compounds have good to moderate antibacterial and antifungal activity against the bacterial and fungal strains. Besides, the ligands and complexes **1** and **3** exhibit selective and effective activity against *Candida* species. Multi-drug resistant microorganisms pose a serious challenge to the medical community and there is therefore an urgent need to develop new agents. In this sense, we think that the ligands and three metal complexes **1**–**3** might be effective as antibacterial and antifungal agents. Thus, the remarkable DNA binding affinity, antibacterial and antifungal activities suggest that the above compounds would have potential application for developing new drugs for cancer.

Acknowledgments

The authors express their sincere thanks to the College Managing Board, Principal and Head of the Department of Chemistry, VHNSN College for providing necessary research facilities and financial support. Instrumental facilities provided by Sophisticated Analytical Instrument Facility (SAIF), IIT Bombay and CDRI, Lucknow are gratefully acknowledged.

Appendix A. Supplementary data

Supplementary data associated with this article can be found, in the online version, at doi:10.1016/j.saa.2011.03.017.

References

[1] B. Lippert, Coord. Chem. Rev. 200–202 (2000) 487–516.
[2] S. Rekha, K.R. Nagasundara, Indian J. Chem. A45 (2006) 2421–2425.
[3] A.R. Banerjee, J.A. Jaeger, D.H. Turner, Biochemistry 32 (1993) 153–163.
[4] J.G. Liu, B.H. Ye, H. Li, Q.X. Zhen, L.N. Ji, Y.H. Fu, J. Inorg. Biochem. 76 (1999) 265–271.
[5] W.Y. Zhong, J.S. Yu, W.L. Huang, K.Y. Ni, Y.Q. Liang, Biopolymers 62 (2001) 315–323.
[6] A.K. Patra, S. Roy, A.R. Chakravarty, Inorg. Chim. Acta 362 (2009) 1591–1599.
[7] A. Vogel, Text Book of Quantitative Inorganic Analysis, third ed., ELBS, Longman, London, 1969.
[8] G. Wilkinson, R.D. Gillard, J.A. McCleverty, Comprehensive Coordination Chemistry, Pergamon Press, Oxford, 1987.
[9] F. Arjmand, B. Mohani, S. Ahmad, Eur. J. Med. Chem. 40 (2005) 1103–1110.
[10] V. Uma, M. Kanthimathi, T. Weyhermuller, B. Unni Nair, J. Inorg. Biochem. 99 (2005) 2299–2307.
[11] M. Sonmez, M. Celebi, I. Berber, Eur. J. Med. Chem. 45 (2010) 1935–1940.
[12] R. Senthil Kumar, S. Arunachalam, Polyhedron 26 (2007) 3255–3262.
[13] B.S. Hammes, C.J. Carrano, J. Chem. Soc., Dalton Trans. 19 (2000) 3304–3309.
[14] A.A. Tak, F. Arjmand, S. Tabassum, Transit. Met. Chem. 27 (2002) 741–747.
[15] A.S. El-Tabl, T.I. Kashar, R.M. El-Bahnasawy, A.E. Ibrahim, Pol. J. Chem. 73 (1999) 245–254.
[16] Q. Yun Chen, H. Jian Fu, J. Huang, R. Xian Zhang, Spectrochim. Acta A 75 (2010) 355–360.
[17] M. Odabasoglu, F. Arslan, H. Olmez, O. Buyukgungor, Dyes Pigments 75 (2007) 507–515.
[18] Z. Chen, Y. Wu, D. Gu, F. Gan, Spectrochim. Acta A 68 (2007) 918–926.
[19] H. Ünver, Z. Hayvali, Spectrochim. Acta A 75 (2010) 782–788.
[20] M. Patil, R. Hoonur, K. Gudasi, Eur. J. Med. Chem. 45 (2010) 2981–2986.
[21] S. Budagumpi, N.V. Kulkarni, G.S. Kurdekar, M.P. Sathisha, V.K. Revankar, Eur. J. Med. Chem. 45 (2010) 455–462.
[22] P.M. Angus, R.J. Geue, N.K.B. Jensen, F.K. Larsen, C.J. Qin, A.M. Sargeson, J. Chem. Soc., Dalton Trans. 22 (2002) 4260–4263.
[23] T.A. Reena, M.R. Prathapachandra Kurup, Spectrochim. Acta A 76 (2010) 322–327.
[24] P. Kamalakannan, D. Venkappayya, Russ. J. Coord. Chem. 28 (2002) 423–433.
[25] F.A. Cotton, G. Wilkinson, Advanced Inorganic Chemistry. A Comprehensive Text, fourth ed., John Wiley and Sons, New York, 1986.
[26] J. Muller, K. Felix, C. Maichle, E. Lengfelder, J. Strahle, U. Weser, Inorg. Chim. Acta 233 (1995) 11–19.
[27] V.P. Daniel, B. Murukan, B. Sindhu Kumari, K. Mohanan, Spectrochim. Acta A 70 (2008) 403–410.
[28] B.J. Hathaway, D.E. Billing, Coord. Chem. Rev. 5 (1970) 143–207.
[29] B.J. Hathaway, Struct. Bond. 14 (1973) 49–67.
[30] V.A. Sawant, B.A. Yamgar, S.K. Sawant, S.S. Chavan, Spectrochim. Acta A 74 (2009) 1100–1106.
[31] J.E. Coury, J.R. Anderson, L. McFail-Isom, L.D. Williams, L.A. Bottomley, J. Am. Chem. Soc. 119 (1997) 3792–3796.
[32] L. Tan, Y. Xiao, X. Liu, S. Zhang, Spectrochim. Acta A 73 (2009) 858–864.
[33] S. Mathur, S. Tabassum, Cent. Eur. J. Chem. 4 (2006) 502–522.
[34] E.K. Efthimiadou, A. Karaliota, G. Psomas, J. Inorg. Biochem. 104 (2010) 455–466.
[35] Y. Jun Liu, C. Hui Zeng, H. Liang Huang, L. Xin He, F. HaiWu, Eur. J. Med. Chem. 45 (2010) 564–571.
[36] A.M. Pyle, J.P. Rehmann, R. Meshoyrer, C.V. Kumar, N.J. Turro, J.K. Barton, J. Am. Chem. Soc. 111 (1989) 3051–3058.
[37] J. Jiang, X. Tang, W. Dou, H. Zhang, W. Liu, C. Wang, J. Zheng, J. Inorg. Biochem. 104 (2010) 583–591.
[38] D. Dong Li, J. Lei Tian, W. Gu, X. Liu, S. Ping Yan, J. Inorg. Biochem. 104 (2010) 171–179.
[39] T. Hirohama, Y. Kuranuki, E. Ebina, T. Sugizaki, H. Arii, M. Chikira, P.T. Selvi, M. Palaniandavar, J. Inorg. Biochem. 99 (2005) 1205–1219.
[40] G. Psomas, J. Inorg. Biochem. 102 (2008) 1798–1811.
[41] K. Jiao, Q.X. Wang, W. Sun, F.F. Jian, J. Inorg. Biochem. 99 (2005) 1369–1375.
[42] N. Raman, A. Kulandaisamy, C. Thangaraja, P. Manisankar, S. Viswanathan, C. Vedhi, Transit. Met. Chem. 29 (2004) 129–135.